Journal of Power Sources 189 (2009) 204–210

Contents lists available at ScienceDirect

Journal of Power Sources

journal homepage: www.elsevier.com/locate/jpowsour

Cobalt oxide thin film prepared by an electrochemical route for Li-ion battery

Jing-Shan Do*, Rui-Feng Dai

Department of Chemical Engineering and Materials Engineering, Tunghai University, Taichung 40704, Taiwan

ARTICLE INFO

Article history:
Received 6 August 2008
Received in revised form
18 September 2008
Accepted 19 September 2008
Available online 4 October 2008

Keywords:
Cobalt hydroxide
Cobalt oxide
Thin film
Anodic material
Lithium battery

ABSTRACT

Cobalt oxide (CoO) thin film was prepared by the calcination of its precursor ($Co(OH)_2$) electrodeposited in the $Co(NO_3)_2$ and $NaNO_3$ aqueous solution. The characteristics of $Co(OH)_2$ and CoO were analyzed by SEM, FTIR and XRD, respectively. The FTIR analysis revealed that the cobalt hydroxide was of the form α-$Co(OH)_2$, which could be converted to β-type by immersing in KOH solution. The pure CoO could be obtained by calcining α-$Co(OH)_2$ at a temperature greater than 500 °C in high purity N_2 atmosphere. Increasing the run number for electrodepositing α-$Co(OH)_2$ from 2 to 6, the weight of α-$Co(OH)_2$ and CoO decreased from 0.913 and 0.700 mg to 0.750 and 0.525 mg due to the decrease in the pH of the electrolyte with the run number. The grain size of CoO decreased from 12.88 to 6.98 nm by decreasing the pH for preparing α-type precursor from 3.30–3.14 to 2.82–2.71. The morphologies of CoO and α-type precursor found from the SEM images were to be nano-fibrillar structures. Using CoO synthesized by calcining α-$Co(OH)_2$ electrodeposited at pH 3.30–3.14 as the cathode, the maximum discharge capacity of Li/CoO coin cell was obtained to be 1589.4 mAh g^{-1}. The irreversible discharge capacity of the Li/CoO coin cells at the first cycle could be recovered in the following activation cycles.

1. Introduction

Lithium-ion battery has been considered as a promising power source for modern electronics due to its highest energy density among commercial rechargeable batteries. The commonly used anodic material in the lithium-ion battery is a carbonaceous compound because of its low cost and high operational voltage. Though the capacity can be improved significantly by the development of highly disordered carbonaceous compounds [1,2], the capacity is still unsatisfied, especially for the thin-film Li-batteries. The high specific capacity is obtained upon using metal alloys [3–8] and metal oxides [9–12] as the anodic materials of lithium-ion battery. Using metal alloys as anodic materials, the decrease in the specific capacity with cycle number due to the pulverization problems associated with the large change of volume during the charge/discharge cycle is still a problem that needs to be solved [3,13]. Metal oxide, such as SnO_2, is developed to overcome the large volume change between the lithiated and lithium-free host. The reversible specific capacity of SnO_2 with good cycle stability is found to be 600 mAh g^{-1} [9]. However, a large irreversible capacity in the first cycle due to the formation of Li_2O prevents the commercialization of tin oxides [13]. In recent years, Co_3O_4 [14–18] and various vanadates [19–22] are also used as the anodic materials in lithium-ion batteries. The relative higher reversible specific capacities are found in these materials, however, the large irreversible capacity in the first cycle and fading rate are needed to be improved for further applications.

Using nano-sized transition metal oxides (MO, where M is Co, Ni, Cu or Fe) as anodes of Li batteries, an insertion-extraction mechanism different from that of carbonaceous compounds or lithium-alloying processes is proposed [14,16,23–27]. The reversible charge/discharge mechanism of CoO was mentioned to be the decomposition of CoO to Li_2O and Co by the insertion of Li^+ [23,28]. The reversible capacity of CoO is obtained to be 600–800 mAh g^{-1} at the room temperature [14,23,25]. Using the homemade CoO powder as the anodic material of lithium-ion battery, the electrochemical and charge/discharge properties of CoO, and the effect of calcination temperature were discussed in our previous papers [29,30].

Thin-film batteries could potentially be applied to the microelectronic mechanical systems (MEMSs), implantable medical devices, integrated circuits with self-power sources, smart cards, and portable electronic devices [31–33]. The charge/discharge properties of miniature Ni-MH batteries prepared by the microfabrication technologies based on the ceramic and polypropylene film substrates have been investigated in our previously works [34,35]. Recently, the lithium and lithium-ion micro-batteries fabricated with the thin-film technologies are also widely reported in the literatures [31–33,36–47]. However, thin-film lithium-ion batteries based on cobalt oxides as anode are seldom reported [47]. A large

* Corresponding author. Tel.: +886 4 23590262x114; fax: +886 4 23590009.
E-mail address: jsdo@thu.edu.tw (J.-S. Do).

0378-7753/$ – see front matter © 2008 Elsevier B.V. All rights reserved.
doi:10.1016/j.jpowsour.2008.09.093

irreversible capacity in the first cycle and a higher fading of capacity are found by using thin-film Co_3O_4 as the anode of lithium-ion battery [47]. In our previous investigations [29,30], a relative lower irreversible discharge capacity is found based on the homemade CoO powder as the anodic material of Li-ion battery in the first cycle, and the irreversible discharge capacity can be recovered in the following charge/discharge cycles. Hence, it is of interest to prepare thin CoO film as the anode of thin-film Li-ion battery.

The CoO thin-film is prepared by the calcination of $Co(OH)_2$ precursor synthesized by the electrolytic deposition. The factors affecting the properties of $Co(OH)_2$, and the characteristics and the charge/discharge properties of CoO thin-film are investigated in this work.

2. Experimental

2.1. Electrodeposition of $Co(OH)_2$ and preparation of CoO

A Cu $4 \times 8\,cm^2$ foil folded to $4 \times 4\,cm^2$ was placed in 0.175 M $Co(NO_3)_2$ and 0.075 M $NaNO_3$ aqueous-ethyl alcohol (v/v ratio of 1) solution as the working electrode for the electrodeposition of $Co(OH)_2$. The edges of the Cu foil were pasted up by some adhesives to obtain the $Co(OH)_2$ deposit on one side of the $4 \times 8\,cm^2$ Cu foil. Two Au plates with the dimension of $5 \times 6\,cm^2$ placed on both sides of the working electrode (Cu foil) were used as the counter electrode, and the Ag/AgCl/3 M NaCl aqueous solution was used as the reference electrode. The $Co(OH)_2$ electrodeposited on Cu foil with a constant current controlled by an electrochemical analyzer (CHI 604) was washed with ethyl alcohol and deionized (DI) water for several times, and then dried at 70 °C in vacuum for 24 h. The obtained $Co(OH)_2$/Cu was cut into eight circular pieces with an area of 1.3 cm^2 and calcined in a tubular oven environed with 99.995% N_2 for 1 h to prepare CoO/Cu.

2.2. Characterization of $Co(OH)_2$ and CoO

The bonding properties of $Co(OH)_2$ were analyzed with a Fourier Transform Infrared (FTIR) Spectrometer (Shimadzu IR Prestige-21). The crystallographic information, grain size and surface morphologies of $Co(OH)_2$/Cu and CoO/Cu were analyzed by X-ray powder diffraction (XRD, Shimadzu XRD-6000) and SEM (Joel JSM-5400).

2.3. Electrochemical and charge/discharge characteristics of CoO

The Li/CoO coin cells were fabricated in a glove-box (VAC MO-5) filled with argon environment described previously [29,30]. The coin cells were galvanostatically charged and discharged at a suitable C-rate, and the voltage behavior against time was recorded over the potential range of 0.02–3.0 V (vs. Li/Li^+). The coin cell was first discharged from the open circuit voltage (OCV) to 0.02 V, and then charged and discharged between 0.02 and 3.0 V in the following cycles.

3. Results and discussion

3.1. Preparation of $Co(OH)_2$/Cu

Using Cu foil as the working electrode for the electrodeposition of $Co(OH)_2$ at the current density (cd) of 0.5 mA cm^{-2}, the cathodic potential sharply increased from −1.1 V to −1.3 V in the initial stage of the first run, and then it decreased slowly to −1.1 V as sown in Fig. 1. The electrochemical reactions on the Cu foil were proposed to be the reduction of NO_3^- [48] and H_2O:

$$NO_3^- + H_2O + 2e^- \rightarrow 2OH^- + NO_2^- \quad (1)$$

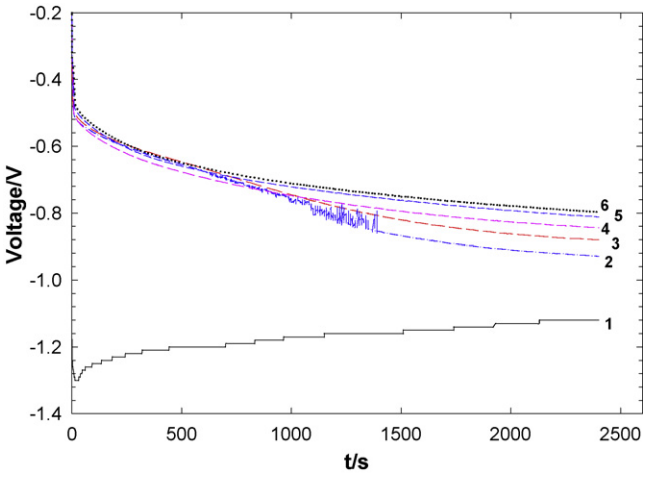

Fig. 1. Effect of electrolysis time on the voltage for electrodeposition of $Co(OH)_2$. Working electrode: Cu foil ($4 \times 4\,cm^2$); counter electrode: Au plate ($5 \times 5\,cm^2$) × 2; reference electrode: Ag/AgCl/3 M NaCl aqueous solution; cd = 0.5 mA cm^{-2}; T = 5 °C; electrolyte: 0.175 M $Co(NO_3)_2$, 0.075 M $NaNO_3$ aqueous and ethyl alcohol solution (v/v = 1); volume of electrolyte = 250 ml.

$$2H_2O + 2e^- \rightarrow H_2 + 2OH^- \quad (2)$$

Hence the significant increase in the cathodic potential from −1.1 to −1.3 V was mainly caused by establishing the diffusion boundary layer on the cathodic surface. The hydroxide ion (OH^-) produced in Eqs. (1) and (2) was deposited with Co^{2+} in the solution onto the Cu foil. At the same time, the increase in the concentration of H^+ in the solution was due to the anodic oxidation of H_2O on the anode, resulting in a decrease in the solution pH from 5.40 to 3.30 in the first run of electrodeposition (Table 1). The increase in the concentration of H^+ induced the cathodic reduction of H^+ on the cathode, resulting in a decrease in the cathodic potential from −1.3 to −1.1 V (Fig. 1).

$$2H^+ + 2e^- \rightarrow H_2 \quad (3)$$

In the first run of the electrodeposition of $Co(OH)_2$, a non-uniform film was obtained due to the higher $Co(OH)_2$ deposition rate caused by the fast OH^- generation rate based on Eqs. (1) and (2).

The cathodic reaction of H_2O to produce OH^- (Eq. (2)) was generally replaced by the evolution of H_2 (Eq. (3)) for the run number greater than 2 due to the decrease in pH of the solution (Table 1). For the run number greater than 2, the uniform $Co(OH)_2$ deposits

Table 1
Effect of the run number on the preparation of $Co(OH)_2$.

Run no.	pH	Residual Co^{2+} [a] (%)	Weight [b] (mg)	
			α-$Co(OH)_2$	CoO
1	5.40–3.30	99.5	–	–
2	3.30–3.14	99.0	0.913	0.700
3	3.14–2.94	98.5	0.888	0.675
4	2.94–2.82	98.0	0.800	0.575
5	2.82–2.71	97.5	0.763	0.538
6	2.71–2.66	97.0	0.750	0.525

Working electrode: Cu foil ($4 \times 4\,cm^2$); counter electrode: Au plate ($5 \times 5\,cm^2$) × 2; reference electrode: Ag/AgCl/3 M NaCl aqueous solution; cd = 0.5 mA cm^{-2}; T = 5 °C; electrolysis time = 40 min; electrolyte: 0.175 M $Co(NO_3)_2$; 0.075 M $NaNO_3$ aqueous and ethyl alcohol solution (v/v = 1); volume of electrolyte = 250 ml.

[a] Residual Co^{2+} in the solution(%) = ($[Co^{2+}]/[Co^{2+}]_i$) × 100%, where $[Co^{2+}]$ and $[Co^{2+}]_i$ were the concentration of Co^{2+} in the present time and the initial state, respectively.

[b] The average weights were measured based on the eight pieces of the samples with area of 1.327 cm^2.

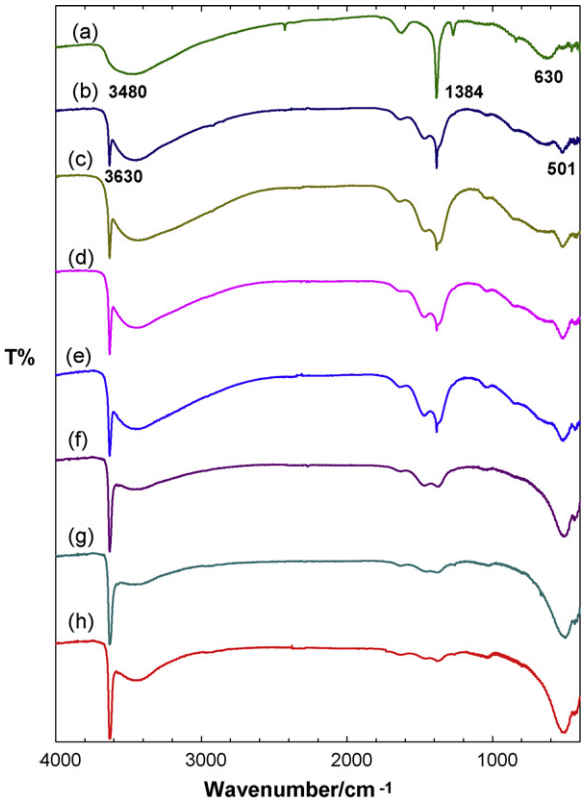

Fig. 2. FTIR spectra of $Co(OH)_2$ electrosynthesized in pH 3.30–3.14 immersed in 1.0 M $KOH_{(aq)}$ with (a) 0; (b) 0.5; (c) 1.0; (d) 1.5; (e) 2.0; (f) 5.0; (g) 10.0; and (h) 15.0 min.

on Cu foil were obtained due to the slower electrodeposition rate caused by the less OH^- generation rate when compared to the first run. Furthermore, the pH and the concentration of Co^{2+} in the solution decreased with the run number, however, the residual concentration of Co^{2+} was still 97.0% of the initial value for the sixth run. Upon increasing the run number from 2 to 6, the weight of $Co(OH)_2$ deposit decreased from 0.913 to 0.750 mg due to the slower deposition rate (Table 1).

3.1.1. Characterization of $Co(OH)_2$

As indicated in Table 1, the pH of the solution for depositing $Co(OH)_2$ was less than 3.30 for the run number greater than 2. Hence, a part of $Co(OH)_2$ deposit would react with H^+ in the solution to form crystal water according to the following reaction:

$$Co(OH)_2 + xH^+ \rightarrow [Co(OH)_{2-x}\cdot(H_2O)_x]^{x+} \quad (4)$$

At the same time NO_3^- was inserted into the structure to compensate for the positive charge of the deposit to form α-type $Co(OH)_2$ [49,50]:

$$[Co(OH)_{2-x}\cdot(H_2O)_x]^{x+} + xNO_3^- \rightarrow Co(OH)_{2-x}(NO_3)_x\cdot y(H_2O) \quad (5)$$

When the as-deposited $Co(OH)_2$ was dried at 70 °C vacuum oven and then analyzed by FTIR, two peaks at 630 and 1384 cm^{-1} were found due to the Co–O and N–O bonds (curve (a) of Fig. 2). The broad feature at 3480 cm^{-1} was deduced to be the O–H stretching with the hydrogen bond. The experimental results revealed that the electrolytic deposit was due to α-$Co(OH)_2$. The synthesis and properties of α-type $Co(OH)_2$ was also reported in the literatures [49,50].

The as-deposited α-$Co(OH)_2$ immersed in 1.0 M KOH aqueous solution for various time periods were washed with DI water for several times, and then dried in a vacuum oven at 70 °C for 24 h. The products were analyzed using FTIR and the spectra are shown in Fig. 2(b)–(h). The strength of 1384 cm^{-1} peak due to the N–O stretching was found to decrease upon increasing the immersion time in 1.0 KOH solution, and disappeared for a time greater than 10 min. On the other hand, the peak strength of 3630 cm^{-1} due to the O–H stretching without hydrogen bond increased with the immersing time as shown in curves (b)–(h) of Fig. 2. The experimental results indicated that replacing NO_3^- in the α-$Co(OH)_2$ by OH^- resulted in a decrease in the peak strength of 1384 and 3480 cm^{-1} peaks, and increase in the 3630 cm^{-1} peak strength by increasing the immersing time. The α-type $Co(OH)_2$ was completely converted to be the β-type for immersion time greater than 10 min. The amount of NO_3^- inserted into the α-$Co(OH)_2$ structure was increased upon decreasing the pH value for electrodeposition, and then the time for replacing NO_3^- by OH^- in the immersion process also increased. The time for completely converting α-$Co(OH)_2$ prepared in the pH range of 2.82–2.71 to its β-type was experimentally found to be 20 min.

3.1.2. Effect of pH

The nano-fibrillar structures were found from the SEM images of α-$Co(OH)_2$ electrosynthesized under various pH values as shown in Fig. 3. The anisotropic growth of the deposit along with one crystal orientation resulted in the nano-fibrillar structure. The structures of cobalt hydroxides had been demonstrated by XRD analysis [48], and the nanorod structure of cobalt-hydroxide-carbonate was also reported in the literature [51]. A relative rougher nano-fibrillar structure with diameter of 30–40 nm was obtained for α-$Co(OH)_2$ prepared at a higher pH (3.30–3.14) (Fig. 3(a)). Upon decreasing the solution pH, the electrodeposition rate of α-$Co(OH)_2$ was decreased due to the lower generation rate of OH^- from the cathode, and resulted in a decrease in the diameter of the nanofiber (Fig. 3(b) and (c)). When α-$Co(OH)_2$ prepared at a pH of 3.30–3.14 and 2.82–2.71 were immersed in 1.0 M KOH aqueous solution for 10 and 20 min, respectively, to convert α-$Co(OH)_2$ to its β form, a part of nano-fibrillar structure of α-$Co(OH)_2$ were collapsed due to the replacement of NO_3^- by OH^- (Fig. 4).

3.2. Preparation and characterization of CoO/Cu

The CoO could be prepared by the calcination of cobalt hydroxide in a high purity of N_2 atmosphere. However, the NO_3^- doping ion present in the α-$Co(OH)_2$ played the role of oxidant to oxidize CoO to Co_3O_4 at a temperature of 300 °C [50]. When the α-$Co(OH)_2$ was calcined in N_2 atmosphere at 300 °C, the pure Co_3O_4 phase was obtained and demonstrated in the XRD spectra (Fig. 5). The intercalation ion NO_3^- was found to be completely released from α-$Co(OH)_2$ structure for a temperature greater than 350 °C [50]. When the calcination temperature was increased to 400 °C, a part of Co_3O_4 was decomposed to CoO by releasing oxygen, and hence formed the mixing phases of Co_3O_4 and CoO as illustrated in the curve (c) of Fig. 5. The pure phase of CoO was obtained at a calcination temperature greater than 500 °C (Fig. 5(d) and (e)).

When the α-$Co(OH)_2$ precursors prepared at various pH were calcinated in 500 °C in 99.995% N_2 for 1 h, pure CoO phase was obtained. The CoO phase was confirmed by the XRD spectra (curves (a)–(c) of Fig. 6). The average grain size was calculated based on the Sherrer equation at 2θ of 36.5 and 42.4° corresponding to the crystal orientation planes of (1 1 1) and (2 0 0), respectively. The grain size of CoO based on (1 1 1) orientation plane decreased from 12.88 to 6.98 nm upon decreasing the pH for preparing its precursor (α-type $Co(OH)_2$) from 3.30–3.14 to 2.82–2.71 (Table 2). The NO_3^- inserted into the structure of the deposit was increased upon decreasing the pH of solution for preparing α-$Co(OH)_2$, and the amount of oxygen evolved during the decomposition of Co_3O_4 to CoO in the calcina-

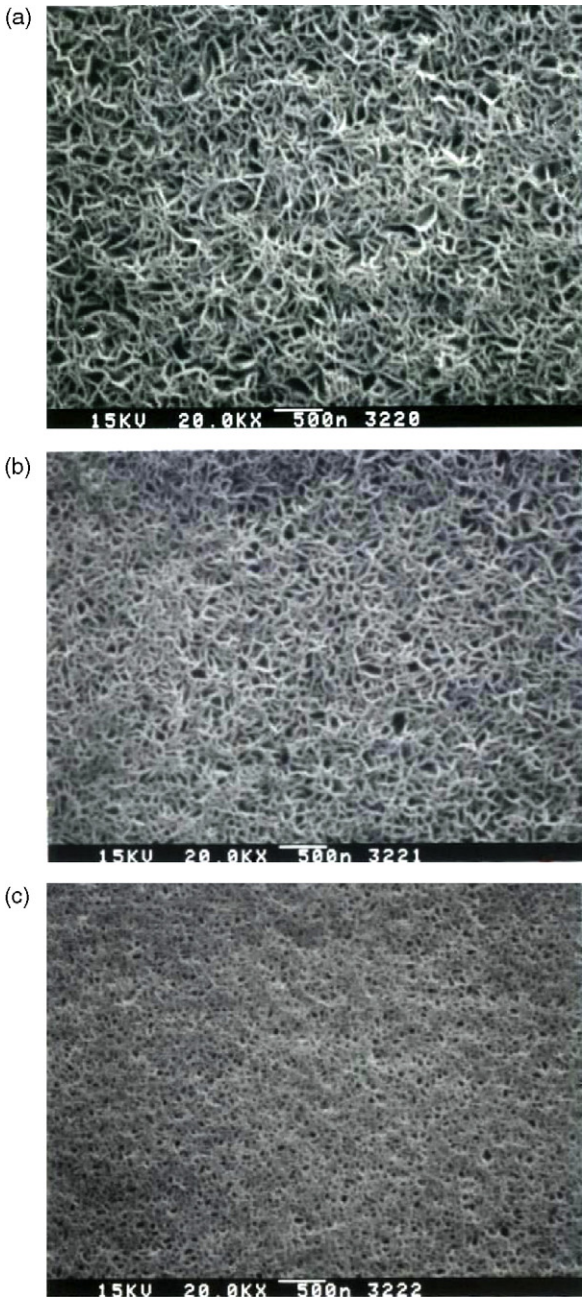

Fig. 3. SEM images of α-$Co(OH)_2$/Cu prepared at pH of (a) 3.30–3.14; (b) 2.94–2.82; (c) 2.71–2.66. Working electrode: Cu foil ($4 \times 4\,cm^2$); counter electrode: Au plate ($5 \times 5\,cm^2$) × 2; reference electrode: Ag/AgCl/3 M NaCl aqueous solution; cd = 0.5 mA cm^{-2}; $T = 5\,^{\circ}C$; electrolyte: 0.175 M $Co(NO_3)_2$; 0.075 M $NaNO_3$ aqueous and ethyl alcohol solution (v/v = 1); volume of electrolyte = 250 ml; electrolysis time = 40 min.

Table 2
Effect of pH for preparing α-$Co(OH)_2$ on the grain size of CoO.

pH for preparing precursor	Grain size of CoO (nm)	
	(1 1 1)	(2 0 0)
2.82–2.71	6.98	7.61
2.94–2.81	8.68	7.10
3.30–3.14	12.88	12.18

Conditions for preparing α-$Co(OH)_2$: working electrode: Cu foil ($4 \times 4\,cm^2$); counter electrode: Au plate ($5 \times 5\,cm^2$) × 2; reference electrode: Ag/AgCl/3 M NaCl aqueous solution; cd = 0.5 mA cm^{-2}; $T = 5\,^{\circ}C$; electrolyte: 0.175 M $Co(NO_3)_2$; 0.075 M $NaNO_3$ aqueous and ethyl alcohol solution (v/v = 1); volume of electrolyte = 250 ml, t = 40 min. Conditions for calcining $Co(OH)_2$: $T = 500\,^{\circ}C$; temperature increasing and decreasing rate = 5 °C min^{-1}; t = 1 h; 99.995% N_2.

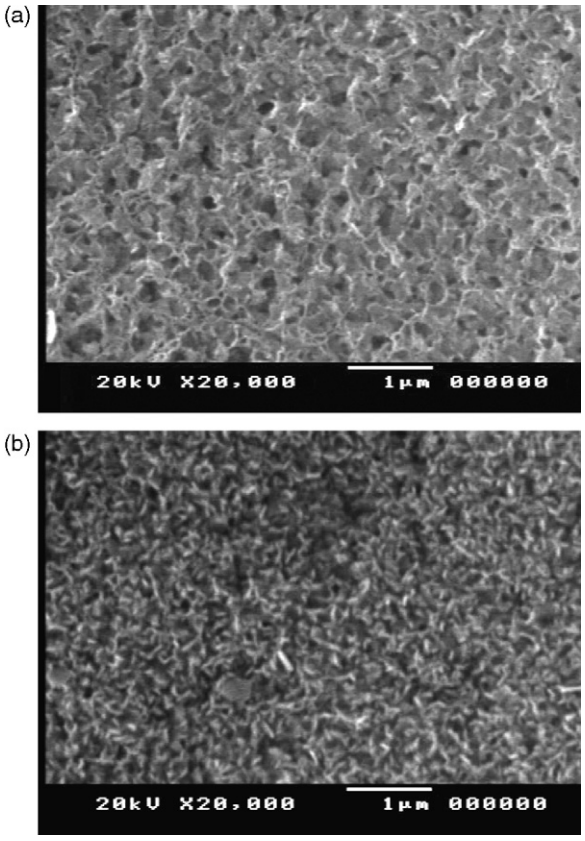

Fig. 4. SEM images of β-$Co(OH)_2$/Cu prepared at pH of (a) 3.30–3.14 and immersed in 1.0 M $KOH_{(aq)}$ for 10 min; (b) 2.82–2.71 and immersed in 1.0 M $KOH_{(aq)}$ for 20 min. Working electrode: Cu foil ($4 \times 4\,cm^2$); counter electrode: Au plate ($5 \times 5\,cm^2$) × 2; reference electrode: Ag/AgCl/3 M NaCl aqueous solution; cd = 0.5 mA cm^{-2}; $T = 5\,^{\circ}C$; electrolyte: 0.175 M $Co(NO_3)_2$; 0.075 M $NaNO_3$ aqueous and ethyl alcohol solution (v/v = 1); volume of electrolyte = 250 ml; electrolysis time = 40 min.

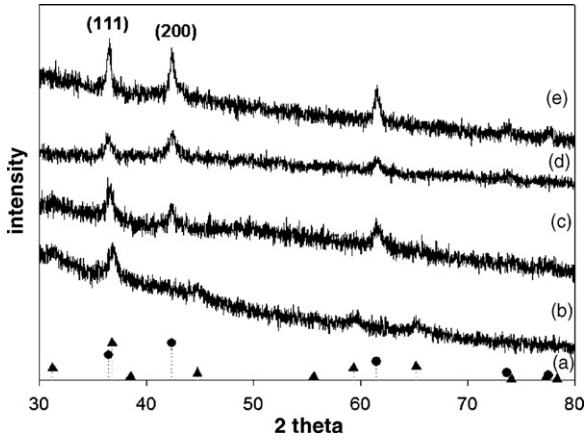

Fig. 5. XRD spectra of cobalt oxides prepared by the calcination of α-$Co(OH)_2$/Cu in the various temperatures. Conditions for preparing α-$Co(OH)_2$: working electrode: Cu foil ($4 \times 4\,cm^2$); counter electrode: Au plate ($5 \times 5\,cm^2$) × 2; reference electrode: Ag/AgCl/3 M NaCl aqueous solution; cd = 0.5 mA cm^{-2}; $T = 5\,^{\circ}C$; electrolyte: 0.175 M $Co(NO_3)_2$; 0.075 M $NaNO_3$ aqueous and ethyl alcohol solution (v/v = 1); volume of electrolyte = 250 ml; pH 3.30–3.14; t = 40 min. Conditions for calcinating α-$Co(OH)_2$: temperature increasing and decreasing rate = 5 °C min^{-1}; t = 1 h; 99.995% N_2. (a) JCPDS data of CoO (●) and Co_3O_4(▲); calcination temperature of (b) 300; (c) 400; (d) 500; and (e) 600 °C.

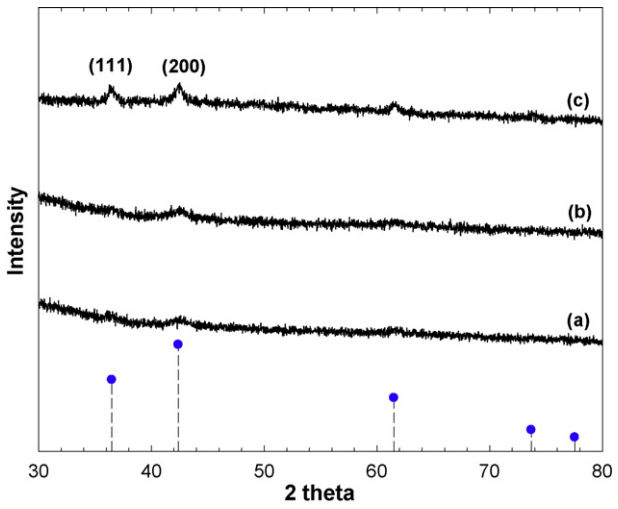

Fig. 6. XRD spectra of cobalt oxides prepared by the calcination of α-$Co(OH)_2$/Cu prepared at pH of (a) 2.82–2.71; (b) 2.94–2.84; (c) 3.30–3.14. Conditions for preparing α-$Co(OH)_2$: working electrode: Cu foil ($4 \times 4\,cm^2$); counter electrode: Au plate ($5 \times 5\,cm^2$) × 2; reference electrode: Ag/AgCl/3 M NaCl aqueous solution; cd = 0.5 mA cm^{-2}; T = 5 °C; electrolyte: 0.175 M $Co(NO_3)_2$; 0.075 M $NaNO_3$ aqueous and ethyl alcohol solution (v/v = 1); volume of electrolyte = 250 ml; t = 40 min. Conditions for calcining $Co(OH)_2$: T = 500 °C; temperature increasing and decreasing rate = 5 °C min^{-1}; t = 1 h; 99.995% N_2. (●) JCPDS of CoO.

tions process was increased. Hence the grain size of CoO decreased with the pH for preparing the precursor of CoO (α-$Co(OH)_2$).

The nano-fibrillar structure of CoO prepared by the calcination of α-$Co(OH)_2$ was found from the SEM images in Fig. 7(a)–(c), which were similar with its precursors (α-type) as indicated in Fig. 3. The results revealed that the main structure of α-$Co(OH)_2$ was not affected in the calcining procedure. The porosity of the nano-fibrillar structure of CoO decreased with the pH of the solution for preparing α-type precursor.

3.3. Charge/discharge characteristics of CoO/Cu

The charge/discharge rate of Li/CoO battery was calculated based on the theoretical capacity of CoO multiplied by the actual weight of CoO thin film on the Cu foil substrate. The theoretical discharge capacity of CoO was obtained to be 715.4 mAh g^{-1} based on the following charge/discharge process [23]:

$$CoO + 2Li^+ + 2e^- \rightleftharpoons Li_2O + Co \quad (6)$$

Using CoO/Cu prepared at pH of 3.30–3.14 as cathode, the discharge potential of CoO/Li coin cell sharply decreased from the OCV (2.704 V) to 0.86 V at 0.1 C rate which corresponded to the discharge capacity of 200 mAh g^{-1} (Fig. 8). The discharge mechanism of CoO/Li in the initial period of first cycle demonstrated by the oxygen K-edge XAS spectra was inferred to the formation of solid electrolyte interface on the CoO surface, and the valence of Co was unchanged [28]. The discharge plateau in the range of 0.86–0.72 V in the first cycle corresponded with the capacity of 715 mAh g^{-1}. This was deduced to be the reduction of CoO to Co as indicated in Eq. (6), which was accompanied with the decomposition of CoO grain size from 12.88 nm (Table 2) to about 1–2 nm [23]. The decrease in discharge potential from 0.72 to 0.02 V corresponding to the capacity of 433.1 mAh g^{-1} was attributed to the formation of polymer/gel-like film [26,27]. Cobalt was re-oxidized to CoO in the first charge cycle, but the particle size of CoO was remained in 1–2 nm. The discharge plateau for the reduction of CoO (Eq. (6)) was increased to 2.0–1.0 V in the second discharge cycle. Compared with the first discharge cycle, the significant increase in the discharge plateau

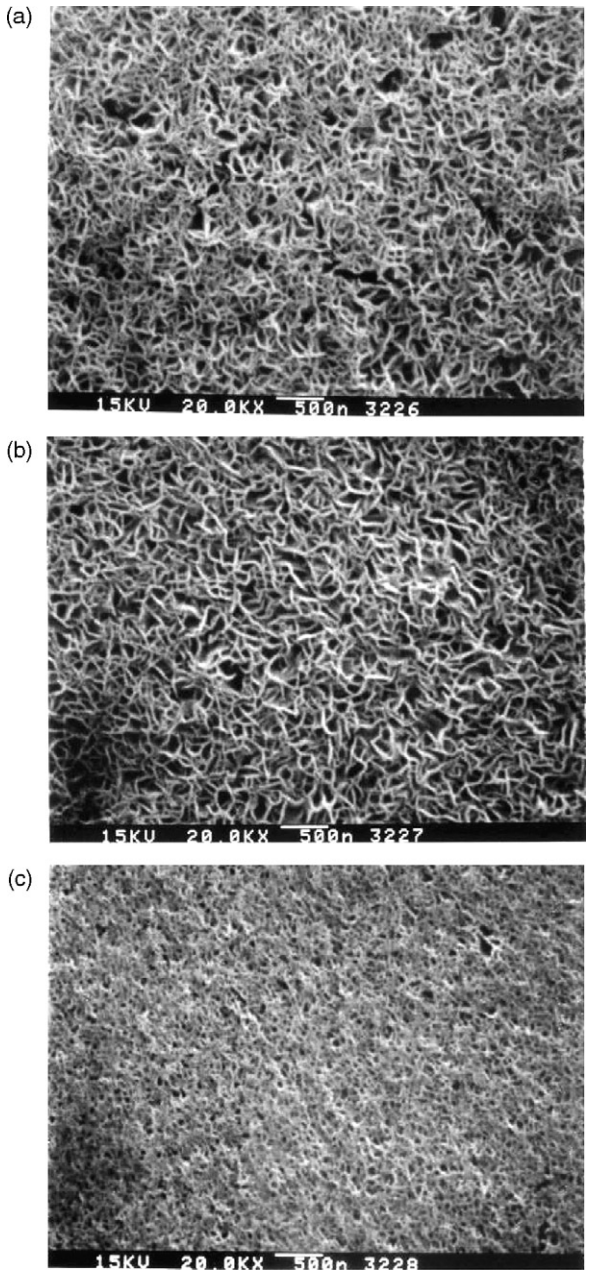

Fig. 7. SEM images of CoO/Cu prepared by calcinating α-$Co(OH)_2$ electrodeposited at pH of (a) 3.30–3.14; (b) 2.92–2.82; (c) 2.82–2.71.

potential was due to the significant decrease in the particle size of CoO. Furthermore, the formation of solid electrolyte interface in the first discharge cycle was not found in the second discharge cycle. The decrease in discharge capacity from 1348.1 to 1089.2 mAh g^{-1} by increasing the cycle number from 1 to 2 was mainly caused by the absence of the formation of solid electrolyte interface, and partially caused by the decrease in the reduction of CoO (Eq. (6)) as shown in Fig. 8.

As shown in Fig. 9, when the precursor of CoO (α-$Co(OH)_2$) was prepared at pH 3.30–3.14, the discharge capacity of Li/CoO coin cell increased from 1089.2 mAh g^{-1} to a maximum value of 1589.4 mAh g^{-1} with the increase in the cycle number from 2 to 25, which was defined as the activation period. As indicated in the discharge curve (Fig. 8) with cycle number of 30, the increase in the discharge capacity as compared with the results in the cycle

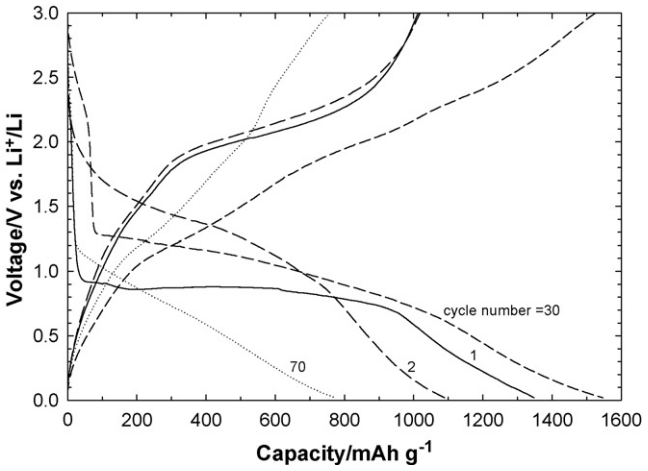

Fig. 8. Charge/discharge curves of Li/CoO coin cell. Conditions for preparing α-$Co(OH)_2$: cd = 0.5 mA cm^{-2}; pH 3.30–3.14; t = 40 min. Calcination conditions for preparing CoO: T = 500 °C; t = 1 h; 99.995% N_2. Conditions for coin cell: cathode: CoO/Cu; anode: Li foil; 1.0 M $LiPF_6$ in EC-DEC (1:1). Charge/discharge conditions: charge/discharge rate = 0.1 C; first discharge cycle: OCV to 0.02 V; other cycles: 0.02–3.0 V; T = 30 °C.

number of 2 was mainly contributed by increasing the capacity for forming polymer/gel-like film. The discharge capacity of polymer/gel-like film increased from 418.2 to 752.4 mAh g^{-1} by increasing the cycle number from 2 to 30 (Fig. 8). The results indicated that the irreversible capacity in the first cycle could be completely recovered in the activation period. The stable discharge capacity could be obtained for the cycle number between 25 and 40. However, the discharge capacity decreased from 1555.1 to 774.7 mAh g^{-1} with the increase in the cycle number from 40 to 70 (Fig. 9). The decrease in the discharge capacity for the cycle number greater than 40 was found to be caused by the decrease in the capacity based on the reduction of CoO (Eq. (6)) as indicated in the discharge curve with cycle number of 70 in Fig. 8. The results might be due to the increase in the diffusion resistance of Li^+ through the polymer-gel formed on the surface of the CoO/Co and Li_2O cluster.

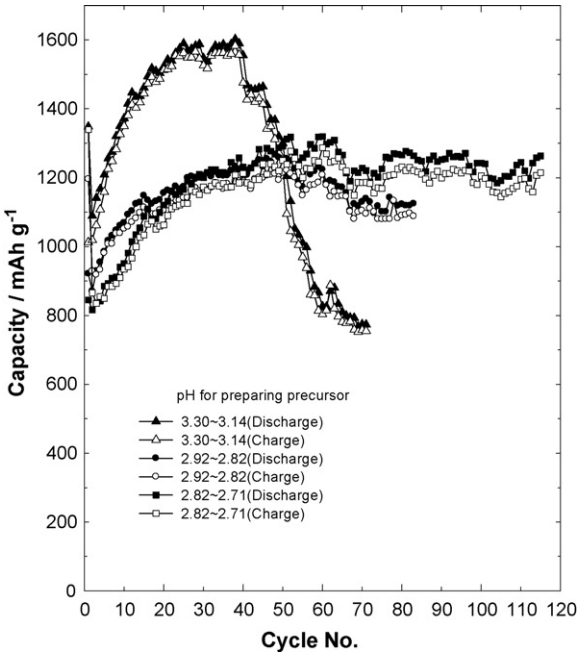

Fig. 9. Effect of charge/discharge cycle number on the capacity of Li/CoO coin cell. Conditions for preparing α-$Co(OH)_2$: cd = 0.5 mA cm^{-2}; t = 40 min. Calcination conditions for preparing CoO: T = 500 °C; t = 1 h; 99.995% N_2. Conditions for coin cell: cathode: CoO/Cu; anode: Li foil; 1.0 M $LiPF_6$ in EC-DEC (1:1). Charge/discharge conditions: charge/discharge rate = 0.1 C, first discharge cycle: OCV to 0.02 V; other cycles: 0.02–3.0 V; T = 30 °C.

When the precursor α-$Co(OH)_2$ of CoO were prepared at pH of 2.92–2.82 and 2.82–2.71, the charge/discharge behaviors of Li/CoO coin cells were similar to that the precursor prepared at pH 3.30–3.14. The activation periods were also found for the precursor of CoO prepared at pH 2.92–2.82 and 2.82–2.71 (Fig. 9). The results in Fig. 9 also revealed that the fading in the discharge capacity with the cycle number for the precursor of CoO prepared at pH 2.92–2.82 and 2.82–2.71 was significantly less than that of prepared at pH 3.30–3.14. As illustrated in Table 1, the weight of α-$Co(OH)_2$ was decreased upon decreasing the pH for preparing α-$Co(OH)_2$, and therefore the weight and thickness of the CoO thin film also decreased. Therefore, when the pH for preparing the precursor of CoO increased, the increase in the electric resistance of CoO film due to its poor conductivity resulted in the decrease in the reversible capacity and the increase in the capacity fading of the Li/CoO coin cell.

The discharge capacity of Li/CoO coin cell was slightly greater than that of the charge capacity as shown in Fig. 9. The limiting capacity electrode of Li/CoO cell investigated of this work was CoO, i.e. the capacity of CoO electrode was significantly less than that of the Li foil electrode. In the every cycle of charge/discharge process, the Li/CoO coin cell was firstly discharged and followed by the charge process. On the other hand, for the CoO electrode, the charge process was firstly taken place and then followed by the discharge process. Hence the discharge capacity of Li/CoO cell was slightly larger than the charge capacity.

4. Conclusions

The characteristics of CoO thin film and its precursor ($Co(OH)_2$), which was electrodeposited on Cu foil by the constant current method at various pH values were analyzed by XRD, FTIR and SEM, respectively. The pH of the solution for electrodepositing cobalt hydroxide decreased from 5.40 to 2.66 by increasing the run number from 1 to 6. The uniform $Co(OH)_2$ deposits obtained for the run number greater than 2 were demonstrated to be α-type ($Co(OH)_{2-x}(NO_3^-)_x{\cdot}y(H_2O)$) by the FTIR spectra. Pure Co_3O_4, mixture of Co_3O_4 and CoO, and pure CoO phases were obtained at calcining temperatures of 300 °C, 400 °C and greater than 500 °C, respectively, under a high purity N_2 atmosphere. Increasing the run number for preparing α-$Co(OH)_2$ from 2 to 6, the weight of α-$Co(OH)_2$ and CoO decreased from 0.913 and 0.700 mg to 0.750 and 0.525 mg due to the decrease in the pH of electrolyte for electrodepositing α-$Co(OH)_2$. The grain size of CoO decreased from 12.88 to 6.98 nm with the decrease in the pH for preparing α-$Co(OH)_2$ from 3.30–3.14 to 2.82–2.71. The morphology of α-$Co(OH)_2$ changed slightly in the calcination procedure, and the nano-fibrillar structure was found for both α-$Co(OH)_2$ and CoO. When CoO prepared by calcining α-$Co(OH)_2$ electrodeposited at pH 3.30–3.14 was used as the cathode, the maximum discharge capacity of Li/CoO coin cell was obtained to be 1589.4 mAh g^{-1}, which was contributed by the formation of solid electrolyte interface, the reduction of CoO and the formation of polymer/gel-like film, respectively. The irreversible discharge capacity of the Li/CoO coin cells at the first cycle could be recovered in the following activation cycles.

Acknowledgment

Financial support from the National Science Council Republic of China (Project number: NSC 96-2120-M-011-001) and Tunghai University is acknowledged.

References

[1] K. Sato, M. Noguchi, A. Demachi, N. Oki, M. Endo, Science 264 (1994) 556–558.
[2] J.R. Dahn, T. Zheng, Y. Liu, J.S. Xue, Science 270 (1995) 590–593.
[3] M. Winter, J.O. Besenhard, Electrochim. Acta 45 (1999) 31–50.
[4] O. Mao, J.R. Dahn, J. Electrochem. Soc 146 (1999) 414–422.
[5] K.D. Kepler, J.T. Vaughey, M.M. Thackeray, J. Power Sources 81–82 (1999) 383–387.
[6] G.X. Wang, L. Sun, D.H. Bradhurst, S. Zhong, S.X. Dou, H.K. Liu, J. Alloys Compd. 306 (2000) 249–252.
[7] O. Crosnier, T. Brousse, X. Devaux, P. Fragnaud, D.M. Schleich, J. Power Sources 94 (2001) 169–174.
[8] X.B. Zhao, G.S. Cao, C.P. Lv, L.J. Zhang, S.H. Hu, T.J. Zhu, B.C. Zhou, J. Alloys Compd. 315 (2001) 265–269.
[9] Y. Idota, T. Kubota, A. Matsufuji, Y. Maekawa, T. Miyasaka, Science 276 (1997) 1395–1397.
[10] I.A. Courtney, J.R. Dahn, J. Electrochem. Soc. 144 (1997) 2045–2052.
[11] J. Read, D. Foster, J. Wolfenstine, W. Behl, J. Power Sources 96 (2001) 277–281.
[12] F. Belliard, J.T.S. Irvine, J. Power Sources 97–98 (2001) 219–222.
[13] B. Scrosati, Electrochim. Acta 45 (2000) 2461–2466.
[14] F. Badway, I. Plitz, S. Grugeon, S. Laruelle, M. Dollé, A.S. Gozdz, J.-M. Tarascon, Electrochem. Solid-State Lett. 5 (2002) 115–118.
[15] G.X. Wang, Y. Chen, K. Konstantinov, J. Yao, J. Shn, H.K. Liu, S.X. Dou, J. Alloys Compd. 340 (2002) L5–L10.
[16] G.X. Wang, Y. Chen, K. Konstantinov, M. Lindsay, H.K. Liu, S.X. Dou, J. Power Sources 109 (2002) 142–147.
[17] D. Larcher, G. Sudant, J.-B. Leriche, Y. Chabre, J.-M. Tarascon, J. Electrochem. Soc. 149 (2002) A234–A241.
[18] Y.-M. Kang, K.-T. Kim, K.-Y. Lee, S.-J. ee, J.-H. Jung, J.-Y. Lee, J. Electrochem. Soc. 150 (2003) A1538–A1543.
[19] S. Denis, E. Baudrin, M. Touboul, J.-M. Tarascon, J. Electrochem. Soc. 144 (1997) 4099–4109.
[20] E. Baudrin, S. Laruelle, S. Denis, M. Touboul, J.-M. Tarascon, Solid State Ionics 123 (1999) 139–153.
[21] S. Denis, E. Baudrin, F. Orsini, G. Ouvrard, M. Touboul, J.-M. Tarascon, J. Power Sources 81–82 (1999) 79–84.
[22] S. Laruelle, P. Poizot, E. Baudrin, V. Briois, M. Touboul, J.-M. Tarascon, J. Power Sources 97–98 (2001) 251–253.
[23] P. Poizot, S. Laruelle, S. Grugeon, L. Dupont, J.-M. Tarascon, Nature 407 (2000) 496–499.
[24] S. Grugeon, S. Laruelle, R. Herrera-Urbina, L. Dupont, P. Poizot, J.-M. Tarascon, J. Electrochem. Soc. 148 (2001) A285–A292.
[25] S. Grugeon, S. Laruelle, P. Poizot, J-M. Tarascon, U.S. Patent WO 200,171,833 (2001).
[26] S. Laruelle, S. Grugeon, P. Poizot, M. Dollé, L. Dupont, J.-M. Tarascon, J. Electrochem. Soc. 149 (2002) A627–A634.
[27] M. Dollé, P. Poizot, L. Dupont, J.-M. Tarascon, Electrochem. Solid-State Lett. 5 (2002) A18–A21.
[28] H.C. Choi, S.Y. Lee, S.B. Kim, M.G. Kim, M.K. Lee, H.J. Shin, J.S. Lee, J. Phys. Chem. B 106 (2002) 9252–9260.
[29] J.S. Do, C.H. Weng, J. Power Sources 146 (2005) 482–486.
[30] J.S. Do, C.H. Weng, J. Power Sources 159 (2006) 323–327.
[31] C.-H. Park, M. Park, S.-I. Yoo, S.-K. Joo, J. Power Sources 158 (2006) 1442–1446.
[32] D. Golodnitsky, V. Yufitc, M. Nathan, I. Shechtman, T. Ripenbein, E. Strauss, S. Menkin, E. Peled, J. Power Sources 153 (2006) 281–287.
[33] H. Kim, R.C.Y. Auyeung, A. Piqué, J. Power Sources 165 (2007) 413–419.
[34] J.S. Do, S.H. Yu, S.F. Cheng, J. Power Sources 117 (2003) 203–211.
[35] J.S. Do, S.H. Yu, S.F. Cheng, Biosens. Bioelectron. 20 (2004) 61–67.
[36] J.B. Bates, N.J. Dudney, D.C. Lubben, G.R. Gruzalski, B.S. Kwak, X. Yu, R.A. Zuhr, J. Power Sources 54 (1995) 58–62.
[37] S.D. Jones, J.R. Akridge, J. Power Sources 54 (1995) 63–67.
[38] S.D. Jones, J.R. Akridge, Solid State Ionics 86–88 (1996) 1291–1294.
[39] X. Yu, J.B. Bates, G.E. Jellison, F.X. Hart, J. Electrochem. Soc. 144 (1997) 524–532.
[40] P. Birke, W.F. Chu, W. Weppner, Solid State Ionics 93 (1997) 1–15.
[41] N.J. Dudney, B.J. Neudecker, Curr. Opin. Solid State Mater. Sci. 4 (1999) 479–481.
[42] B.J. Neudecker, R.A. Zuhr, J.B. Bates, J. Power Sources 81–82 (1999) 27–32.
[43] J.B. Bates, N.J. Dudney, B. Neudecker, A. Ueda, C.D. Evans, Solid State Ionics 135 (2000) 33–45.
[44] C. Branci, N. Benjelloun, J. Sarradin, M. Ribes, Solid State Ionics 135 (2000) 169–174.
[45] N.J. Dudney, J. Power Sources 89 (2000) 176–179.
[46] W.C. West, J.F. Whitacre, V. White, B.V. Ratnakumar, J. Micromech. Microeng. 12 (2002) 58–62.
[47] H.-C. Liu, S.-K. Yen, J. Power Sources 166 (2007) 478–484.
[48] R.S. Jayashree, P. Vishnu Kamath, J. Mater. Chem. 9 (1999) 961–963.
[49] R.S. Jayashree, P.V. Kamath, J. Mater. Chem. 9 (1999) 961–963.
[50] Z.P. Xu, H.C. Zeng, Chem. Mater. 12 (2000) 3459–3465.
[51] R. Xu, H.C. Zeng, J. Phys. Chem. B 107 (2003) 12643–12649.